Design and Implementation of LVDC Hybrid Circuit Breaker

Riccardo Lazzari and Luigi Piegari, *Senior Member, IEEE*

***Abstract*—In recent years, dc distribution grids have become increasingly popular because of the interest in the diffusion of distributed renewable energy. In this scenario, dc distribution grids are also favored because of the increased use of batteries and power electronic loads. The main limit to the spread of dc grids is their protection devices, which still present several problems. At present, protection devices are represented by traditional mechanical breakers or static electronic components. The first, which interrupt dc currents, have good reliability but need maintenance and have long intervention periods. In contrast, electronic switches are fast and reliable, but they reduce the efficiency because of their voltage drop. In this scenario, some hybrid breakers have been proposed to obtain the advantages of both devices. The previous solutions of hybrid breakers still suffer several critical issues and, usually, are not capable of protecting a system from short circuits without significantly reducing their lifetime. In this paper, a new low-voltage hybrid circuit breaker topology is proposed. The procedure to dimension all of the active and passive components in the device is analyzed, and the effectiveness of the proposed solution is proven by means of experimental results obtained using a prototype.**

***Index Terms*—DC circuit breakers (CBs), fast CBs, hybrid circuit breaker (HCB), LVdc breakers, protection devices.**

I. Introduction

NOWADAYS, the technological progress in the power conversion field and the wide diffusion of renewable energy sources are promoting the implementation of dc distribution grids. This is a growing trend mainly due to the advantages offered by dc grids when compared to ac grids in many applications (e.g., data centers, marine installations, and offshore wind farms) [1]–[6].

However, the implementation of a dc network introduces a complex mix of power converters with significant technical challenges in order to protect and operate the system. DC converters

Manuscript received April 4, 2018; revised June 26, 2018 and August 31, 2018; accepted October 16, 2018. Date of publication October 28, 2018; date of current version May 22, 2019. This work was supported by the Research Fund for the Italian Electrical System under the Contract Agreement between RSE S.p.A., and the Ministry of Economic Development—General Directorate for the Electricity Market, Renewable Energy and Energy Efficiency, Nuclear Energy in compliance with the Decree of March 8, 2006. Recommended for publication by Associate Editor J. Clare. (*Corresponding author: Luigi Piegari.*)

R. Lazzari is with the Power Generation Technologies and Materials Department, Ricerca sul Sistema Energetico, Milan 20134, Italy (e-mail:

be dissipated through a well-suited cooling system. For these reasons, the applications of SSCBs are strictly limited to applications where the fault currents are limited to a fixed rate, a fast OFF-transition is the essential requirement, and the losses are manageable.

There has been a significant interest in combining an MCB with power semiconductor devices to configure so-called hybrid circuit breakers (HCBs) [19], [20]. An HCB combines the very low resistance of an MCB in the ON-state with the fast and arcless transition from the conduction to the blocking state of an SSCB. To do that, a parallel MCB and SSCB combination is used to reduce the arc, which cannot be avoided in the MCB [21]. In general, it is possible to resort to two main techniques: zero-voltage switching (ZVS) and zero-current switching (ZCS) [22]. In the first case, the voltage across the MCB is maintained close to zero during the separation of the contacts, whereas in the second case, the current in the MCB is forced to zero before turning the device OFF.

In [23], Theisen *et al.* presented a ZVS HCB where a power field-effect transistor (FET) was connected in parallel to an MCB and energy absorber. Under normal conditions, the current flows through the MCB, whereas in the case of a fault, the main contacts of the MCB are opened, and the FET is turned ON. When the current level and arc impedance reach an appropriate level, the current flows in the FET, which can finally interrupt this current. The same operation was also used in [24]–[26], where the current commutation to the SSCB was actuated by the arc generated between the contacts of the MCB during the OFF-transition. However, the arc causes erosion of the contacts, resulting in a shorter lifetime and need for maintenance.

To solve the problem of the arc needed for the commutation in the SSCB branch, in [27], Hassanpoor *et al.* proposed the use of an auxiliary commutating switch comprised of one or more semiconductors in series with the MCB. During normal operation, the current flows through an auxiliary commutating switch and MCB in series. When the commutating switch is turned OFF, the current is quickly diverted to the parallel SSCB, and the MCB can be opened with zero current. In this situation, the power dissipation under normal operation is higher than that of a conventional MCB due to the semiconductor auxiliary switch. For this reason, Song *et al.* [28] and Peng *et al.* [29] proposed the use of a low-voltage MOSFET-based commutating switch, composed of a high parallel number of power semiconductor devices, in order to reduce the losses. However, to maintain low commutation losses, a MOSFET with a low breakdown voltage must be chosen. Therefore, the SSCB can be opened only after the MCB to avoid applying the voltage across the hybrid dc breaker to the commutating switch. The realization of such a device and its snubber circuit is not an easy task [27]. In addition, the SSCB must be designed to handle all of the fault current as long as the MCB is open.

Otherwise, the use of ZCS HCBs may avoid the turn-OFF arcing phenomenon through the use of additional resonant components, which allow the reduction of the MCB current to zero. In [30], Zyborski *et al.* proposed a ZCS structure where the main components were a fast MCB opened by an electrodynamic repulsion force, a pre-charged capacitor, two thyristors, and a voltage suppressor. To interrupt a current, one of the thyristors is turned ON, causing the discharge of the capacitor in the opposite direction of the main current and flowing through the MCB. In this way, the current is reduced, and the mechanical contact can be opened at a fast rate with limited arcing. This HCB is one of the most effective presently available low-voltage current-limiting and interrupting devices [20], but has some disadvantages such as an overvoltage on the load after the MCB opens, the impossibility of reducing the current to zero during a fault, and the necessity of an external circuit to pre-charge the capacitor.

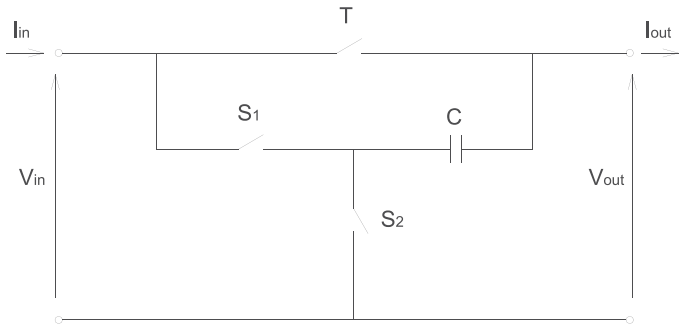

Fig. 1. Basic scheme of the proposed dc breaker.

To solve all these problems, this research aimed to develop a ZCS HCB that is able to switch OFF the circuit during normal operation and during fault condition to avoid an overcurrent and overvoltage on the breaker and dc grid components. The proposed structure can also open on a short circuit using its internal inductances to partially limit the current increase. Moreover, it has a reclosing path for the current to avoid overvoltage on the components. Finally, it integrates all of the necessary devices to pre-charge its capacitor and quickly detect fault conditions.

II. Topology and Working Principle

The basic principle of operation of the proposed dc breaker is explained in the following. In the basic scheme, as shown in Fig. 1, T is a traditional mechanical breaker, whereas S_1 and S_2 are two switching devices (i.e., insulated gate bipolar transistor (IGBT) or MOSFET).

During normal operation in conduction mode, T and S_2 are closed, whereas S_1 is in an open state. In this way, the capacitance C is charged to the supply voltage. In order to open the breaker, S_1 and S_2 are switched ON and OFF, respectively (introducing the necessary dead time). In this way, capacitor C will force the current in T to zero and then change its direction. If T opens its contacts when the current crosses zero, no arc arises. Then, switch S_1 can be opened, interrupting the load current.

The main goal of the proposed hybrid dc breaker is to achieve the following:

1) high efficiency;
2) long lifetime;

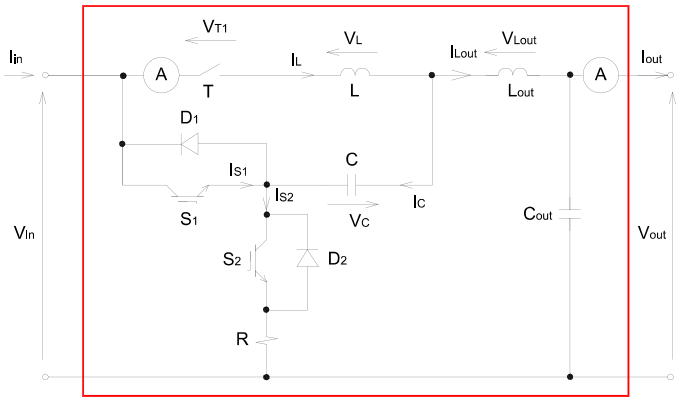

Fig. 2. Complete scheme of the proposed CB.

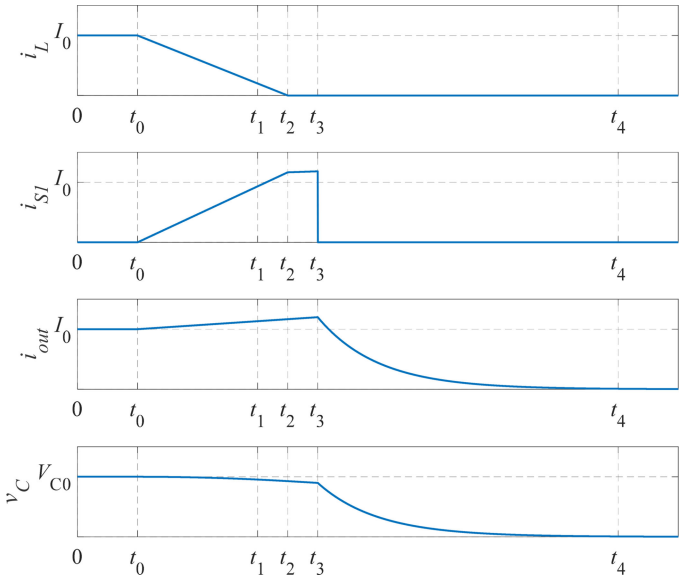

Fig. 3. Working principle of the proposed CB.

3) the ability to open under a short circuit (for the maximum interruption power) without damage.

Point 1 is achieved, by the topology of the breaker shown in Fig. 1, as long as the parasitic resistance in the mechanical breaker T is sufficiently low. In normal operation, the current flows in mechanical device T with negligible voltage drop and power loss. In order to achieve point 2, it is necessary that the opening phases of T are operated at a very low current (possibly in the absence of an arc). With the basic configuration of Fig. 1, it is not possible to ensure this condition. Indeed, when S_1 is turned ON (and S_2 is turned OFF), the current in T quickly becomes negative, making it practically impossible to open with a near zero current. In order to slow down the current inversion, an inductance L is introduced in the scheme in series with the mechanical device T. Moreover, by closing S_1, capacitance C is put in series with the voltage source. For this reason, a voltage that is double the rated one is instantaneously connected to the load, which could cause damage. For this reason, an output inductance L_{out} is used to limit the overvoltage on the load when the breaker opens. Section III will show that the correct sizing of the two inductances allows a current limitation during short circuit for the time necessary to open the circuit. This makes possible the achievement of point 3, allowing the breaker to open, under a short-circuit condition, before the current becomes too high to be interrupted by S_1. In order to quickly identify the fault condition, an output capacitance C_{out} is added to provide a high fault current while the output inductor current is still low. The complete circuit of the proposed breaker is shown in Fig. 2. The parasitic resistances of the two inductances L and L_{out} during normal operation cause additional losses. This point will be addressed as part of the experimental analysis, in Section V-C, where it is shown that losses during normal operation are significantly lower than an all-electronic breaker.

Looking at the scheme of Fig. 2, three other elements can be noted: the resistance R and the two diodes D_1 and D_2. Resistance R is necessary to dissipate the energy stored in capacitance C in the case of a short circuit. When S_1 completes the opening phase of the breaker, capacitance C is still charged. It discharges on the load by means of diode D_2. In the case of a short circuit, a current limitation can be achieved by means of the proper sizing of R, as discussed in Section III. When the breaker is energized, the presence of the capacitance C could cause an overload on the voltage source. In order to limit the charge current, a pulsewidth modulation (PWM) technique is performed on switch S_2 using inductance L to limit the current ripple. During PWM, when S_2 is turned OFF, the inductive current closes in diode D_1, avoiding overvoltage on the two electronic switches.

The complete working principle of the breaker is illustrated in Fig. 3 and summarized as follows.

[t_0–t_1]: At time t_0, the control system decides to open. This could be driven by an opening request from the operator or from a short-circuit detection. At t_0, switch S_2 is opened and, after the necessary dead time, S_1 is closed. The current in S_1 starts increasing while the current in L starts decreasing. If capacitance C is large enough, its voltage is almost constant during this time, and the currents in both S_1 and L change linearly. At time t_1, the current in L reaches a low current threshold, for which the opening of T can be started.

[t_1–t_2]: At time t_1, the opening command to T is sent. T starts opening, and its current reaches zero at time t_2. During this time interval, nothing changes in the circuit.

[t_2–t_3]: After opening the breaker, an additional time interval, t_2–t_3, is introduced before opening S_1. The reason for this delay is that the time needed for the MCB to open could slightly change with aging. During this time, the current in S_1 becomes equal to the output current and increases slower than in the previous intervals.

[t_3–t_4]: At time t_3, switch S_1 is turned OFF. Capacitance C discharges itself on the load with a time constant depending on the series of the load resistance and breaker resistance R. After five times the time constant, the transient can be considered terminated, and the circuit can be considered turned OFF.

In practical implementation, the mechanical breaker requires a not negligible time to open its contacts. In particular, a delay occurs between the instant when the opening command is generated and the instant in which the contacts are detached. If this period is known (for example, by means of

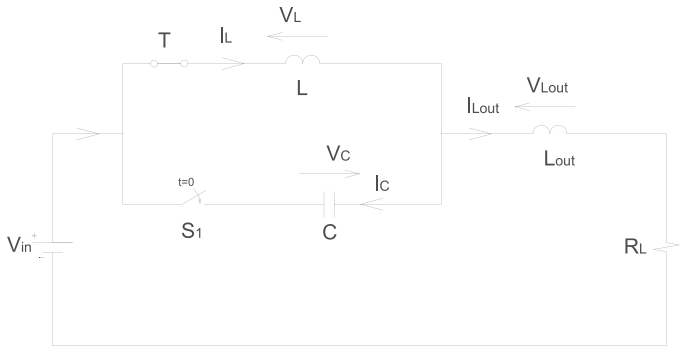

Fig. 4. Electric circuit during opening.

experimental measurements), it is possible to anticipate the command signal of the mechanical breaker, and the working principle remains unchanged. Unfortunately, this delay is not constant but can vary from a minimum to a maximum value in the lifetime of the mechanical breaker. For this reason, a slight modification of the control strategy is implemented in order to keep all the advantages of the proposed solution. In particular, calling t_d the minimum delay, the opening signal of the mechanical device is anticipated by t_d. As a consequence, when the current in the mechanical device becomes zero, the contacts do not open yet and, therefore, the currents become negative and start increasing in the opposite direction. In order to avoid the need to interrupt a high negative current, S_1 is controlled with a hysteresis band to keep the current in a predefined bandwidth around zero. In this way, when the contacts of the mechanical device open, they have to interrupt a very low current.

III. Sizing Procedure

This section proposes a sizing procedure for the passive components of the suggested CB. The components to be sized are the two inductances *L* and L_{out}, the capacitance *C*, and the resistance *R*. At the end of this section, some considerations about the sizing of the switching components will also be given.

In order to correctly size the components, it is possible to analyze the circuit during the opening phase. In the scheme shown in Fig. 4, the output capacitance has been neglected because, as stated above, it is a small capacitance necessary only for tripping purposes.

The resistive load, indicated by R_L, could represent the short-circuit resistance, in the case of opening in a fault condition. The transient can be analyzed by applying Kirchhoff's laws

$$\begin{cases} V_{\text{in}} = L\dfrac{di_L}{dt} + L_{\text{out}}\dfrac{di_{L_{\text{out}}}}{dt} + R_L i_{L_{\text{out}}} \\ V_C + L\dfrac{di_L}{dt} = 0 \\ i_L = i_{L_{\text{out}}} + C\dfrac{dV_C}{dt}. \end{cases} \tag{1}$$

Easily, (1) can be summarized in

$$V_{\text{in}} = L_{\text{out}}LC\frac{d^3 i_L}{dt^3} + R_L LC\frac{d^2 i_L}{dt^2} + (L + L_{\text{out}})\frac{di_L}{dt} + R_L i_L. \tag{2}$$

The system is a third-order system, and it cannot be solved in a closed form. In any case, the worst condition occurs during faults with low impedance. In this case, it is possible to neglect the terms in which R_L appears, and (2) can be rewritten as follows:

$$V_{\text{in}} = L_{\text{out}}LC\frac{d^3 i_L}{dt^3} + (L + L_{\text{out}})\frac{di_L}{dt}. \tag{3}$$

Considering that at the beginning of the phenomenon, the inductive currents are equal to the healthy load current and the capacitance voltage is equal to the source voltage, the initial conditions to be coupled to (3) can be calculated as follows:

$$\begin{cases} i_L(0) = \dfrac{V_{\text{in}}}{R_n} \\ \dfrac{di_L}{dt}(0) = \dfrac{V_L(0)}{L} = -\dfrac{V_C(0)}{L} = -\dfrac{V_{\text{in}}}{L} \\ \dfrac{d^2 i_L}{dt^2}(0) = \dfrac{1}{L}\dfrac{dV_L}{dt}(0) = -\dfrac{1}{L}\dfrac{dV_C}{dt}(0) \\ \quad = -\dfrac{1}{LC} i_C(0) = -\dfrac{1}{LC}\left[i_L(0) - i_{L,\text{out}}(0)\right] = 0 \end{cases} \tag{4}$$

where R_n indicates the load resistance before the fault. Taking into account (4), the solution of (3) can be written in the following form:

$$i_L(t) = \frac{V_{\text{in}}}{R_n} + \frac{V_{\text{in}}}{L + L_{\text{out}}}t - \frac{V_{\text{in}}(2L + L_{\text{out}})}{L(L + L_{\text{out}})}\sqrt{\frac{LL_{\text{out}}C}{L + L_{\text{out}}}}\sin\left(\sqrt{\frac{L + L_{\text{out}}}{LL_{\text{out}}C}}t\right). \tag{5}$$

The current given by (5) increases linearly with some smoothed sinusoidal oscillation, as illustrated in Fig. 5.

In order to allow the inversion of the current in the mechanical component *T,* it is necessary that the first minimum of the function is lower than zero. This condition is expressed by the following equation:

$$\begin{aligned} t^* &= \frac{\pi}{2}\sqrt{\frac{L\,L_{\text{out}}C}{L + L_{\text{out}}}} \\ i_L(t^*) &= \frac{V_{\text{in}}}{R_n} + \frac{V_{\text{in}}}{L + L_{\text{out}}}\frac{\pi}{2}\sqrt{\frac{L\,L_{\text{out}}C}{L + L_{\text{out}}}} \\ &\quad - \frac{V_{\text{in}}(2L + L_{\text{out}})}{L(L + L_{\text{out}})}\sqrt{\frac{L\,L_{\text{out}}C}{L + L_{\text{out}}}} < 0. \end{aligned} \tag{6}$$

From inspecting the second part of (6), it is clear that the input voltage has no effect on the possibility to invert the current. This condition can be ensured with the proper sizing

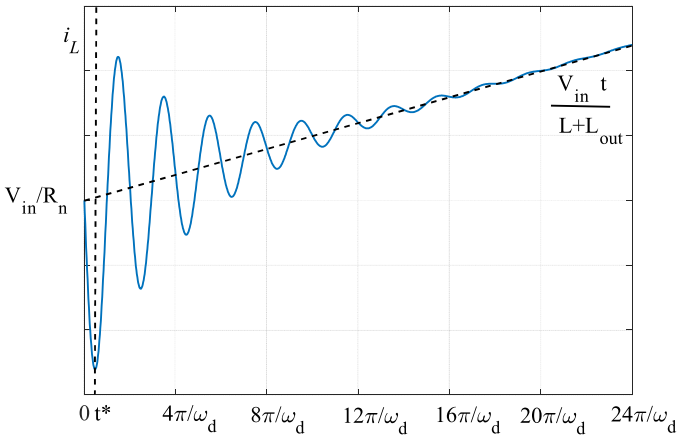

Fig. 5. Trend for the current as given by (6).

of the passive components. Equation (6) can be rewritten as follows:

$$\left(2-\frac{\pi}{2}\right)^2+\left(\frac{L_{\text{out}}}{L}\right)^2+(4-\pi)\frac{L_{\text{out}}}{L}>\frac{(L+L_{\text{out}})^3}{R_n^2 L\, L_{\text{out}} C}. \quad (7)$$

Then, considering a new variable x given by the ratio between L_{out} and L, the result is the following:

$$\begin{aligned} x &= \frac{L_{\text{out}}}{L} \\ f(x) &= \left(R_n^2 C - L\right)x^3 + \left[R_n^2 C(4-\pi) - 3L\right]x^2 \\ &\quad + \left[R_n^2 C\left(2-\frac{\pi}{2}\right)^2 - 3L\right]x - L > 0. \end{aligned} \quad (8)$$

The function $f(x)$ is a cubic whose limit for x that goes to infinite has the sign of the first term. For this reason, a solution always exists if it is

$$R_n^2 C - L > 0 \quad \Rightarrow \quad \frac{L}{C} < R_n^2. \quad (9)$$

If all the coefficients of the polynomial function $f(x)$ are positive, but the last one $f(x)$ is an increasing monotone function and, over a fixed value of x, the second of (8) is always verified. In order to have all the coefficients of the second part of (8) positive, it has to be

$$R_n^2 C(4-\pi) - 3L > 0 \quad \Rightarrow \quad \frac{L}{C} < \frac{R_n^2(4-\pi)}{3}. \quad (10)$$

For each value of *L/C,* it is possible to obtain the minimum value of the ratio L_{out}/L allowing the inversion of the current in *T*. The results are shown in Fig. 6.

The sizing of the passive components also has to take into account the maximum current in switch S_1. Indeed, S_1 has to be capable of conducting and interrupting the current without failing. As discussed in Section II, the current in S_1 increases differently in the two intervals $[t_0–t_2]$ and $[t_2–t_3]$. According to Fig. 3, in the first of the two intervals, it increases with a high slope, the sum of the slopes of $-i_L$ and of i_{out}, whereas in the second interval, it increases with the slope of L_{out}. At the end of

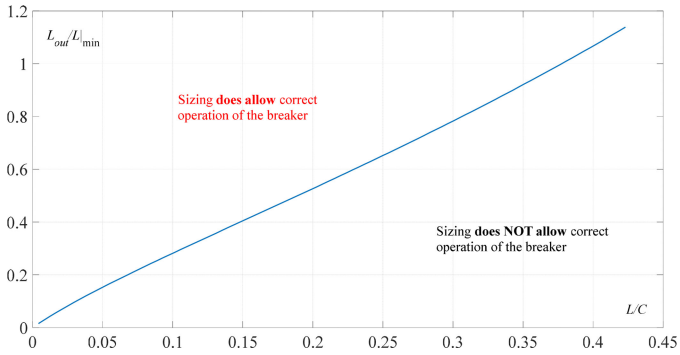

Fig. 6. Minimum ratio L_{out}/L versus ratio *L/C* for correct operation of breaker.

the first interval, it reaches the value I_0, which is the current of the mechanical device when S_1 is turned ON. It is worth noting that, if the breaker is operating in a faulty condition, during the time delay t_d, the current in the mechanical device increases almost linearly, limited by the two inductances L and L_{out} in series. During this transient, we can consider the voltage across the capacitance to be constant, and for a zero load voltage (short circuit) it is found as follows:

$$\begin{cases} \dfrac{di_{S_1}}{dt} = -\dfrac{di_L}{dt} + \dfrac{di_{L_{\text{out}}}}{dt} \approx \dfrac{V_{\text{in}}}{L} + \dfrac{2V_{\text{in}}}{L_{\text{out}}} & t \in [t_0 - t_2] \\ \dfrac{di_{S_1}}{dt} = \dfrac{di_{L_{\text{out}}}}{dt} \approx \dfrac{2V_{\text{in}}}{L_{\text{out}}} & t \in [t_2 - t_3]. \end{cases} \quad (11)$$

The maximum current in the switching device is reached at time t_3 and it is found as follows:

$$I_{s_1,\max} = I_0 + \frac{2V_{\text{in}}}{L_{\text{out}}}(t_3 - t_2). \quad (12)$$

As mentioned above, in the case of a short circuit, during the time delay t_d, the current in the mechanical device increases almost linearly, and it results in the following:

$$I_0 = I_{\text{Load}} + \frac{V_{\text{in}}}{L + L_{\text{out}}} t_d + \frac{2V_{\text{in}}}{L_{\text{out}}}(t_2 - t_0). \quad (13)$$

Combining (12) and (13) results in the following:

$$I_{S_1,\max} = I_{\text{Load}} + \frac{V_{\text{in}}}{L + L_{\text{out}}} t_d + \frac{2V_{\text{in}}}{L_{\text{out}}}(t_3 - t_0). \quad (14)$$

Equation (14) was obtained by assuming that the voltage across the capacitance during the considered operation time is constant. In order to verify if this hypothesis can be considered valid, the voltage drop is estimated.

Because the current in the capacitance is equal to the current in S_1, the variation of the voltage across the capacitance can be

estimated as follows:

$$\begin{aligned}\Delta V_c = V_{\text{in}} - V_c(t_3) &= \frac{1}{C}\left\{\int_{t_0}^{t_2}\left(\frac{V_{\text{in}}}{L}+\frac{2V_{\text{in}}}{L_{\text{out}}}\right)(t-t_0)\,dt\right.\\ &\left.+\int_{t_2}^{t_3}\left[\left(\frac{V_{\text{in}}}{L}+\frac{2V_{\text{in}}}{L_{\text{out}}}\right)(t_2-t_0)+\frac{2V_{\text{in}}}{L_{\text{out}}}(t-t_2)\right]dt\right\}\\ &= \frac{1}{C}\left\{\left(\frac{V_{\text{in}}}{L}+\frac{2V_{\text{in}}}{L_{\text{out}}}\right)\frac{1}{2}\Delta t_2^2\right.\\ &\left.+\int_{t_2}^{t_3}\left[\left(\frac{V_{\text{in}}}{L}\right)(t_2-t_0)+\frac{2V_{\text{in}}}{L_{\text{out}}}(t-t_0)\right]dt\right\}\\ &= \frac{1}{C}\left\{\left(\frac{V_{\text{in}}}{L}+\frac{2V_{\text{in}}}{L_{\text{out}}}\right)\frac{1}{2}\Delta t_2^2+\left(\frac{V_{\text{in}}}{L}\right)\Delta t_2(\Delta t_3-\Delta t_2)\right.\\ &\left.+\frac{V_{\text{in}}}{L_{\text{out}}}(\Delta t_3^2-\Delta t_2^2)\right\}\\ &= \frac{1}{C}\left\{\frac{V_{\text{in}}}{L}\Delta t_2\left(\Delta t_3-\frac{\Delta t_2}{2}\right)+\frac{V_{\text{in}}}{L_{\text{out}}}\Delta t_3^2\right\}\end{aligned} \tag{15}$$

with

$$\begin{aligned}\Delta t_2 &= t_2 - t_0\\ \Delta t_3 &= t_3 - t_0.\end{aligned} \tag{16}$$

According to (16), Δt_2 and Δt_3 represent the time necessary to bring the current to zero in the mechanical device and the time necessary to have the contacts of the breaker far enough apart.

Finally, in order to have a voltage variation on the capacitance lower than a maximum value $\Delta V_{C,\max}$, it has to be as follows:

$$C > \frac{V_{\text{in}}}{\Delta V_{C,\max} L}\Delta t_2\left(\Delta t_3-\frac{\Delta t_2}{2}\right)+\frac{10}{L_{\text{out}}}\Delta t_3^2. \tag{17}$$

Equations (14) and (17) and Fig. 6 give the necessary information to size all the components of the device. An example is reported in Section IV, in which the real prototype is analyzed.

It is worth noting that if inductances with iron cores are used, saturation could occur during short circuit. In this case, the global inductance would decrease affecting the correct operation of the breaker in short-circuit opening. A correct sizing of the inductances should take into account this aspect.

IV. Experimental Test Setup

The capabilities of the proposed HCB were verified through experimental activities carried out on the prototype shown in Fig. 7. The components of the prototype were chosen by considering a nominal voltage of 200 V, nominal current of 20 A, and maximum value of 400 A for the current of the component S_1.

The dc contactor Tyco EV200AAANA was used to realize the prototype. This component, as reported in the datasheet, has a release time (arcing included) equal to 12 ms. In our prototype, the extinguishment of the arc was performed by the suggested structure, and so some preliminary experiments were carried out on the mechanical breaker to evaluate the release time before the arc. The opening time was typically equal to 3.7 ms. Taking into account this information, it was possible to calculate the values of the two inductances L and L_{out}, which satisfied (14). In particular, considering a ratio between L_{out} and L equal to k, it is possible to write the following:

$$L = \frac{V_{\text{in}} k t_d + 2V_{\text{in}}(k+1)\Delta t_3}{(I_{S_1,\max} - I_{\text{Load}})k(k+1)}. \tag{18}$$

Considering an ON-state duration for the component S_1, $\Delta t_3 = 100\ \mu$s, load current $I_{\text{load}} = 20$ A; maximum current in S_1, $I_{S1,max} = 400$ A; and dc voltage $V_{\text{in}} = 200$ V, through (18) it was possible to draw the graph of Fig. 8 considering different values for ratio k.

Therefore, to satisfy this requirement, it is necessary for the total inductance to be about 2 mH. In the realization of the prototype, an inductance L of 400 μH and inductance L_{out} of 1.8 mH were chosen. These inductances modify the behavior of the overall dc grid increasing the total line inductance and reducing the oscillation frequency. In particular, eigenvalues approach the imaginary axis from the left-half plane, decreasing the stability margin of the system. This issue can be approached

Fig. 7. Photograph of the hybrid dc CB prototype.

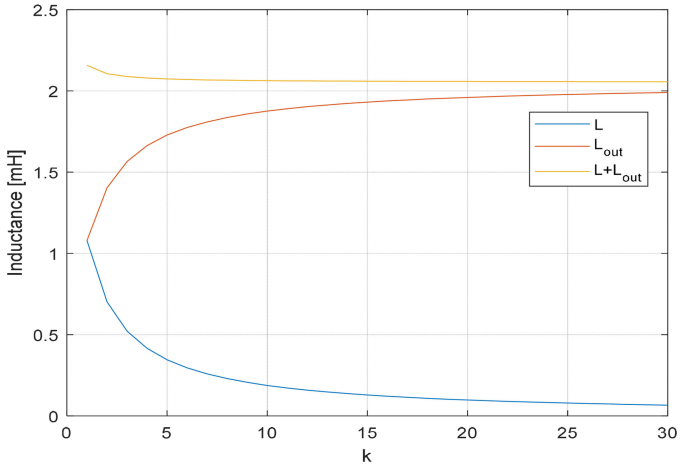

Fig. 8. Trend of inductance values to maintain $I_{S1} < 400$A with input voltage of 200 V in the presence of short circuit.

through the design of the current and voltage controller of the converters in accordance with the stability analysis of the overall grid [31], [32]. However, the use of inductors can limit fault current rating, preventing the fault current to reach the blocking level in the converter and enable the discrimination of the faults in fast protection methods, such as rate of change of voltage (ROCOV) [33].

It is worth noting that the necessity of big inductances is due to the use of a mechanical breaker spending almost 4 ms to open its contacts. By using faster mechanical breakers (that have to work with low currents), the inductances and thereby the losses can be strongly reduced. Fast mechanical dc breakers are under study in recent years and some prototypes, capable of opening in time windows shorter than 4 ms, are presented in [34] and [35].

Starting from the inductances, it was possible to evaluate capacitance C and find a value that satisfied both (9) and (17). Taking into account a maximum voltage variation $\Delta V_{C,\max} = 10\%$, the minimum capacitance was equal to 4 mF, and in the realization of the prototype, a 9.6 mF capacitance was used.

The dimensioning procedure has been set up with a zero fault resistance, so that, for any fault resistance the current is limited by the inductances into a range of correct operability of the device. Nevertheless, if the fault resistance is very low, the initial current, supplied by the output capacitor, could persist over the threshold for a time too short to allow a correct detection. In order to avoid this problem, a correct dimensioning of the output capacitance has to be performed. In particular, the output capacitance must ensure that the current after one control period is still higher than the threshold. Considering a resistive short circuit whose value is R_f, neglecting the current supplied by the output inductance, the fault current can be written as follows:

$$I_{\text{out}} = \frac{V_{\text{in}}}{R_f} e^{-\frac{t}{R_g C_{\text{out}}}}. \tag{19}$$

Imposing that after a control time the output current is higher than the threshold implies

$$\begin{aligned} \frac{V_{\text{in}}}{R_f} e^{-\frac{T_s}{R_f C_{\text{out}}}} &> I_{\text{th}} \\ \frac{T_s}{R_f C_{\text{out}}} &< -\ln\left(I_{\text{th}} \frac{R_f}{V_{\text{in}}}\right) \\ C_{\text{out}} &> \frac{T_s}{R_f \ln\left(\frac{V_{\text{in}}}{R_f I_{\text{th}}}\right)}. \end{aligned} \tag{20}$$

In the prototype, the output capacitance was dimensioned to open a short circuit of 10 kA corresponding to a fault resistance equal to 20 mΩ. The capacitance resulting from the third relation of (20), considering the parameter of the experimental setup, is 97 μF and a 100 μF was used in the prototype. In Fig. 9, the $I_{\text{out}}(T_s)$, evaluated using (19), is compared with the current threshold for different fault resistances with an output capacitance equal to 100 μF. It is clear that, with the used capacitance, the fault can be identified until a minimum resistance around 19.4 mΩ [according with (20)].

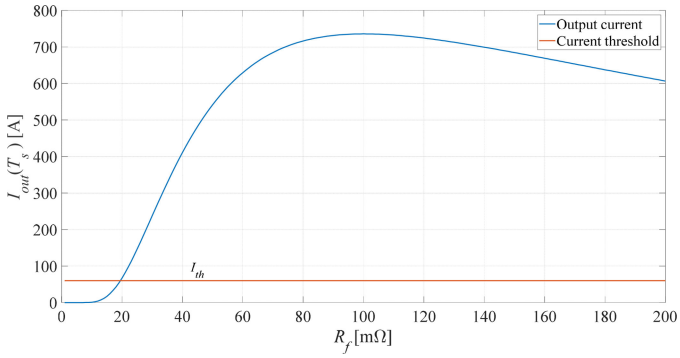

Fig. 9. Output current after one control period versus fault resistance.

TABLE I
HYBRID DC CB PARAMETERS

Component	Specification
Mechanical Breaker T	Tyco EV200AAANA
Switch S1 & S2	Semikron SKM400GB12T4
C	9.6 mF
L	400 µH
Cout	100 µF
Lout	1.8 mH
R	0.5 Ω

It is worth noting that the presence of a big inductance in the fault could slightly change the behavior of the proposed breaker. Indeed, for the presence of the fault inductance the initial peak current could not go over the threshold, triggering the opening of the breaker. In this case, the fault would be identified only when the current in L_{out} reaches the threshold.

The slope of the current in this case would be lower because the fault inductance is in series with the output inductance of the breaker and, therefore, the two effects compensate themselves. A complete analysis of this phenomenon is not in the focus of the paper and will be addressed in future works.

The parameters of all the components of the HCB are summarized in Table I.

The prototype was equipped with two current sensors (LEM HAS 400-S), connected as shown in Fig. 2, and one voltage sensor (LEM LV 25-1000), which was necessary for the pre-charge of C. All these measurements were used by a microcontroller Texas Instruments TMS320F28335PGFA to control the HCB consisting of the mechanical breaker and electronic switches. The realized firmware had a cycle time of 10 μs, and during this time it acquired the output current and eventually activated the start-up or opening procedure if the switching button was pressed by the operator or the current was higher than a fixed threshold. The start-up procedure was realized by closing breaker T and then activating the pre-charge of capacitor C. This was done through electronic switch S_2, which was controlled through a hysteresis control on the capacitor current. When the voltage on capacitor C reached 90% of the input voltage, this procedure finished, and switch S_2 remained closed. During the opening procedure, which could be caused by an external command or a fault detection (the current threshold was set equal

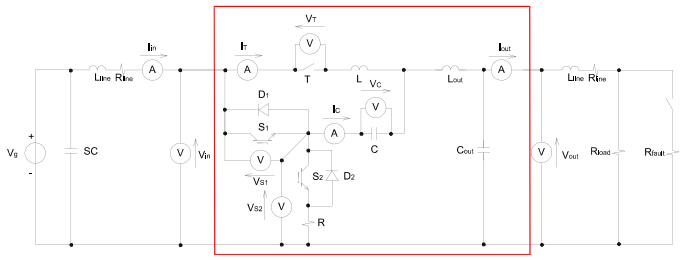

Fig. 10. Experimental test setup.

to 60 A for the prototype), the control after a delay equal to 3.2 ms sent the trip command to mechanical breaker *T,* turn-OFF command to S_2, and switching command to component S_1. The switching command for component S_1 was realized through the use of a hysteresis control to maintain the mechanical breaker current close to zero. After a delay of 3 ms, component S_1 was turned OFF. In this situation, the load was supplied only by capacitor *C*, which was discharged.

V. Experimental Results

The experimental validation of the proposed HCB was performed using the dc microgrid of RSE [36] at a constant voltage of 200 V and connecting the HCB to a dedicated resistive load of 11 Ω. In this study, the experimental activity is focused to verify the ability of the proposed HCB during load interruption and fault interruption with a limited fault current. In particular, a short-circuit fault was simulated with a resistance of 2 Ω. In order to increase the current capacity during the fault, a bank of supercapacitors was installed in parallel with the voltage generator during the test. In the test, an oscilloscope (Tektronix DPO3014) equipped with two voltage probes (Tektronix P5200) was used. For the current measurements, the oscilloscope was directly connected to the current sensor (LEM HAS 400-S) of the prototype. In Fig. 10, the experimental test setup with indicated measurement points is shown.

A. Resistive Load Interruption Test

The performance of the HCB was first verified during a resistive load interruption. Fig. 11 shows the current and voltage of component *T* during an interruption test. At time $t = 0$ ms, the mechanical breaker is closed, S_1 is opened, S_2 is closed, and in this situation, capacitor *C* is connected in parallel to the input source. At time $t_1 = 1.4$ ms, the opening button is pressed, and a trip command is sent to the mechanical breaker. At time $t_2 = 4.6$ ms, the hysteresis control of the current of the mechanical breaker is activated. Switch S_2 is opened, and switch S_1 is switched ON and OFF in order to maintain the mechanical breaker current in a range near zero. In this way, at time $t_3 = 5.1$ ms, the mechanical breaker can open with a current near zero with a limited arc, and finally, at time $t_4 = 5.6$ ms, the switch S_1 can be opened. During the phase t_2–t_3, the current is provided by capacitor *C*.

Looking at Fig. 12, it is also possible to see that the output voltage and consequently the output current increase dur-

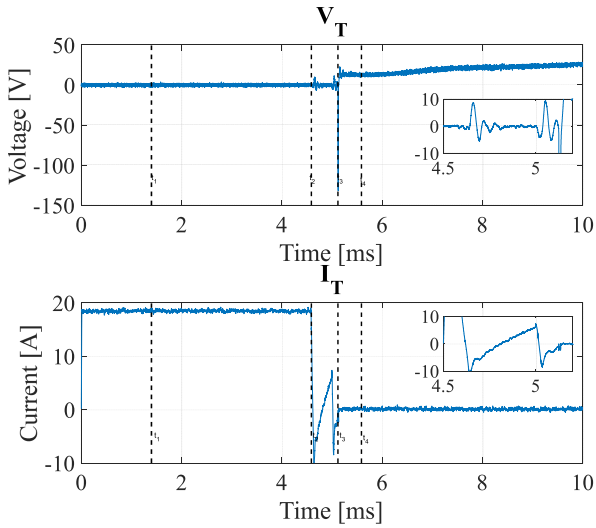

Fig. 11. Resistive load interruption test: mechanical breaker voltage and current.

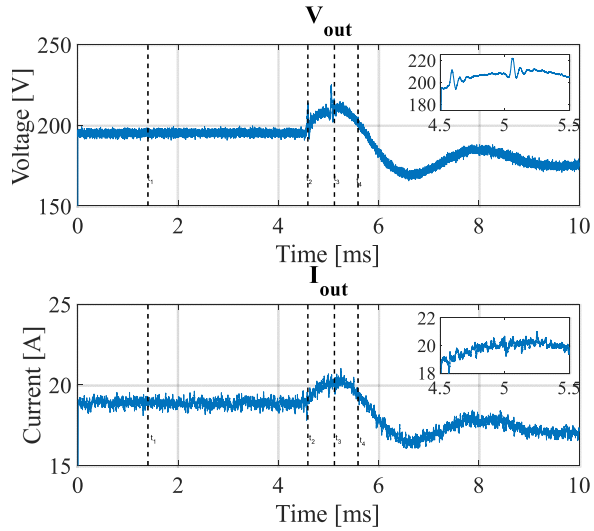

Fig. 12. Resistive load interruption test: load and capacitor current.

ing the phase between t_2 and t_3 because of the insertion of the capacitor *C*. In addition, the switching of the electronic components creates high frequency oscillations on the output voltage that are limited in amplitude. The peak of overvoltage is equal to 225 V that represent only the 12.5% of the nominal voltage.

B. Resistive Fault Interruption Test

The performance of the HCB was also verified during a fault condition. An experiment was performed with the same system configuration described above. The opening command was triggered, in this case, at a preset output current level equal to 60 A. Fig. 13 shows the voltage and current of the MCB. At time $t_1 = 1.75$ ms, the fault is recognized by the control of the HCB, and the sequence presented above is activated. At time

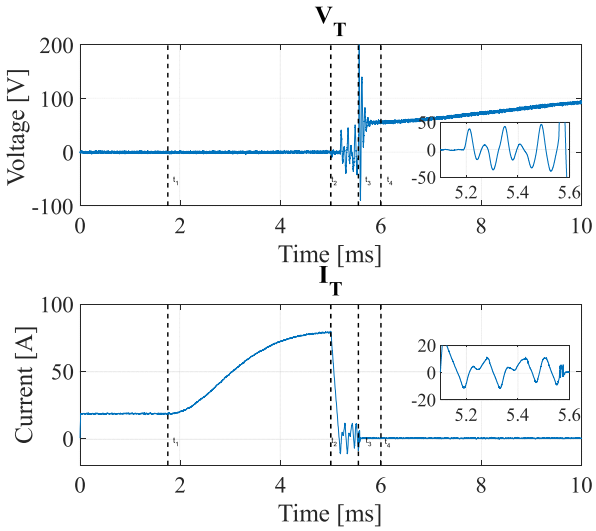

Fig. 13. Resistive fault interruption test: mechanical breaker voltage and current.

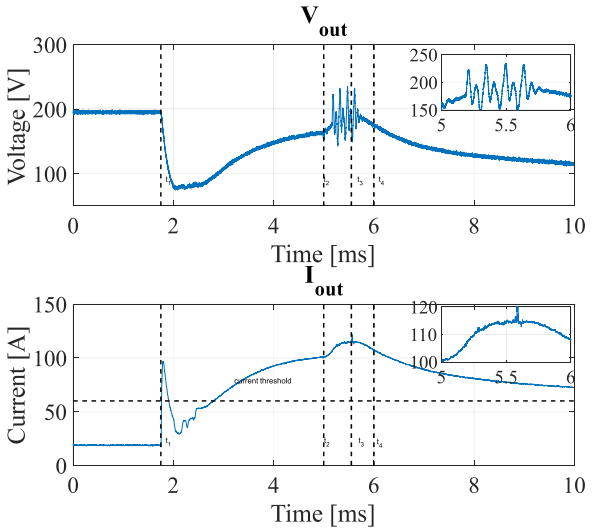

Fig. 14. Resistive fault interruption test: load voltage and current.

$t_2 = 5.00$ ms, switch S_1 starts to modulate, and the current in mechanical breaker T is maintained near zero until it opens its contact at time $t_3 = 5.55$ ms. Starting from this moment, the output current, as shown in Fig. 14, is provided through S_1 until its opening at $t_4 = 6.00$ ms, and then only by the capacitor through diode D_2. After the fault, the output current decreases because of the voltage drop on the inductances. The output capacitor is therefore necessary to provide the initial peak current triggering the opening of the hybrid breaker.

It is worth noting that, also in case of the short circuit, the insertion of the capacitor C and the switching of the component S_1, which create an overvoltage on the output terminal of the HCB, are limited to 16.5% of the nominal voltage. The output voltage oscillation causes only a very small perturbation on the output current since the line and the load have parasitic inductances that limit it.

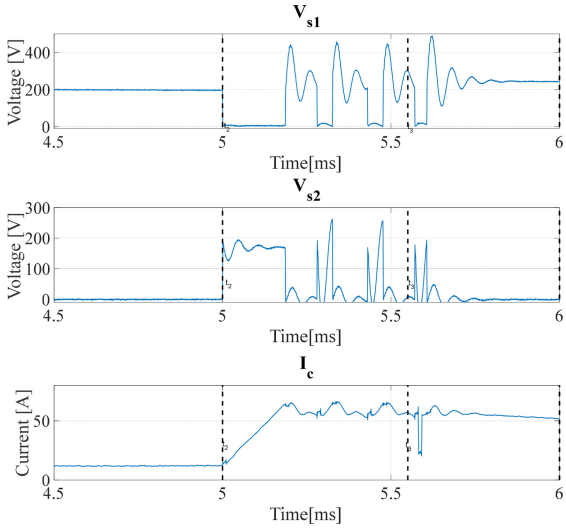

Fig. 15. Resistive fault interruption test: voltage applied to switches S_1 and S_2 and current in capacitor C.

The test results demonstrated that the proposed HCB and its control are also able to operate during a fault with a limited arc on the mechanical breaker. This makes it possible to obtain a long lifetime for this component. In addition, the HCB has the ability to open under a short circuit without damage. The voltage applied to components S_1 and S_2, as shown in Fig. 15, is about two times the nominal voltage of the grid. This overvoltage is due to the parasitic inductance of the input circuit and can be reduced through the use of a capacitance connected in parallel with the input of the breaker. The current flowing through C is equal to the current flowing in the turned-ON switch.

C. Performance Analysis

To analyze the performance of the realized HCB in terms of energy efficiency, additional tests were performed in order to evaluate the internal resistance of the breaker. In the test, the prototype was operated at the nominal voltage and current for 2 h, in order to reach a steady-state temperature. After that, by means of a Power Analyzer Hioki PW3390, the current and the voltage at the input and output ports were measured to estimate the internal resistance of the HCB components, which was 33 mΩ. This resistance is due to the inductance L of 400 μH, which has an internal resistance of 6 mΩ, and to the output inductance L_{out} of 1.8 mH, which presents 27 mΩ of internal resistance. It is worth noting that for the proposed CB, the choice of the mechanical breaker has a strong influence on the losses of the HCB. With a fast MCB, like the one presented in [24], and considering a total breaking time of 1 ms, in order to identify the fault location, the inductance L and L_{out} can be reduced, respectively, to 200 and to 600 μH. In this condition, it is expected that the total resistance reaches values near 10 mΩ.

However, with reference to an SSCB, the conduction losses depend on the type of power semiconductor device used. IGBT is a bipolar device and can be modeled as the series of the ON-state voltage that cause conduction losses. On the other hand,

TABLE II
COMPARISON IN TERMS OF LOSSES BETWEEN THE PROPOSED HCB AND SOME TYPOLOGY OF TRANSISTOR

Component	Manufacturer	Forward Voltage [V]	Internal Resistance [mΩ]	Losses @ 20 A [W]
Hybrid Circuit Breaker	/	/	33	13.2
Hybric Circuit Breaker with a fast MCB [24]	/	/	10	4
Si IGBT SKM 75GB063D	Semikron	1.05	14	26.6
Si MOSFET VS-FA72SA50LC	Vishay	/	80	32
SiC JFET UJN1205K	UnitedSiC	/	45	18
SiC MOSFET SCTWA50N120	STMicroelectronics	/	69	27.6

MOSFET is a unipolar device and the conduction losses depend only on the ON-state resistance. Furthermore, the MOSFET resistance has a positive temperature coefficient and consequently the ON-state resistance increases of two to three times passing from the reference temperature (25 °C) to the maximum temperature. In addition, semiconductor wafer of SSCBs may break down due to overvoltages and overcurrents [26]. This is true in particular for SiC MOSFET that has low short-circuit withstand capability, compared with Si IGBTs and MOSFETs. In particular, the typical short-circuit withstand time of SiC MOSFETs is normally on the order of 1 μs for low-voltage application and 10 μs for medium voltage [37]. This requires a faster response time to guarantee the operation in the safe operation area and avoid overcurrent condition that has negative impact on the long-term stability of the device.

To compare the losses of the proposed HCB with the losses of a comparable electronic CB in Table II, different types of power semiconductor devices (IGBT, Si MOSFET, SiC MOSFET, and SiC JFET), suitable for the voltage and current of the HCB, are collected. As shown in this table, the losses of the proposed HCB are less than the losses of a pure electronic breaker. In particular, considering a fast MCB, the losses are five times less than the losses of the best SSCB.

To verify the performance of the proposed HCB in comparison with the MCB in terms of lifetime, it is necessary to analyze the voltage and the current applied to the mechanical breaker during the interruption test. Figs. 16 and 17 show the trends of voltage and current for the MCB during a load interruption and a fault interruption in the case of HCB and MCB. In the case of MCB, the voltage applied to the mechanical breaker increases to high value during the interruption process and consequently the current decreases, whereas in the case of HCB, the current tends to zero in a very fast way thanks to the switching of S_1 and the voltage is limited to tens of volt. As a consequence, the energy associated to the release of the mechanical breaker in the HCB is much lower than the one of the MCB. In Table III, the energies associated to the interruption processes, dissipated

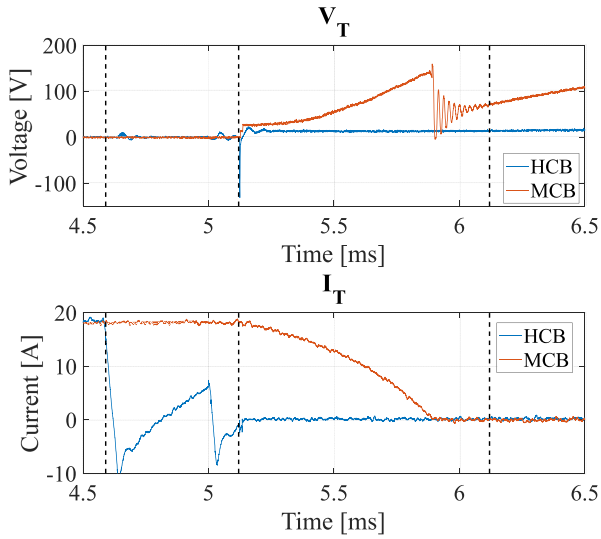

Fig. 16. Resistive load interruption test: Comparison between the voltage and the current in the MCB for the HCB and only the MCB.

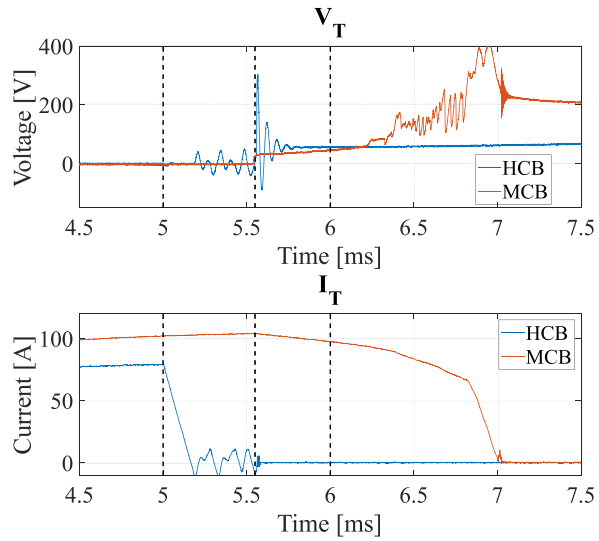

Fig. 17. Resistive fault interruption test: comparison between the voltage and the current in the MCB for the HCB and only the MCB.

TABLE III
COMPARISON BETWEEN THE PROPOSED HCB AND MCB IN TERMS OF ENERGIES DISSIPATED BY THE MECHANICAL BREAKER DURING THE INTERRUPTION PROCESS

	Energy dissipated during the interruption process	
	MCB	HCB
Resistive load interruption of 11 Ω	442.0 mJ	3.3 mJ
Resistive fault interruption of 2 Ω	12200 mJ	14.0 mJ

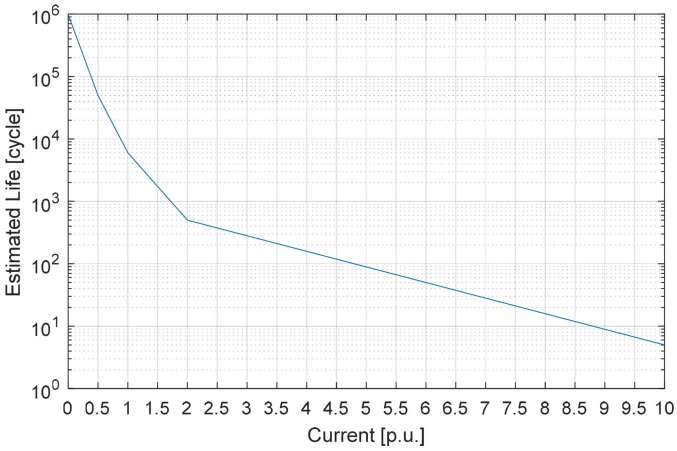

Fig. 18. Lifetime characteristic of the MCB.

by the mechanical breaker, are compared for the MCB and the HCB.

Considering the life characteristic as a function of the current for the adopted MCB [38] shown in Fig. 18, it is possible to evaluate the estimated number of cycles this component can perform in case of HCB and MCB configurations.

For a current equal to the nominal current (20 A), the MCB can perform 6000 cycles, whereas with a current of about 10 A, which is the current threshold in the HCB, the MCB can perform 50 000 cycles. In case of fault interruption with a current of 100 A, the estimated life is about 100 cycles, whereas resorting to the HCB is equal to 50 000 cycles. It is worth noting that the values provided by the manufacturer are related to current interruptions with arc formation. The proposed HCB however reduces the arc time and consequently the energy dissipated by the mechanical breaker. This put in evidence that the expected lifetime of the mechanical breaker used in the HCB could be higher than the values provided by the manufacturers.

VI. Conclusion

In recent years, several studies have been conducted dealing with protection devices for low-voltage dc systems. The solutions can be divided in the following three categories:

1) those based on mechanical improvements to extinguish the electric arc;
2) those consisting of the use of innovative electronic switches with very low voltage drops;
3) those that use hybrid topologies, including static and mechanical breakers.

In this paper, an innovative topology for a hybrid low-voltage dc breaker was proposed. In the proposed solution, a conduction operation is achieved by means of a fast mechanical breaker, ensuring a very low voltage drop and consequent low conduction losses. In contrast, the opening maneuver is achieved by activating an electronic power switch that keeps the current in the mechanical breaker close to zero until this last one opens its contacts. In this way, the mechanical device has to break a very low current with reduced or no-formation of an arc, and consequently a very long lifetime. The proposed topology is designed to also operate correctly in the case of a short circuit. In this case, it is capable of limiting the rising of the current (due to the short circuit) for the whole time necessary to complete the opening operation. In this way, the proposed hybrid dc breaker can be used to protect any device and, in particular, power electronic converters that are not overloadable.

In this paper, a new topology was proposed, and its working principle was theoretically analyzed. Then, the dimensioning of all the components of the device was studied to make the breaker capable of also working in the case of a short circuit. Finally, the results of experimental tests performed on a dedicated prototype were presented and discussed. It was found to be opportune to use very fast mechanical breakers to reduce the size and weight of each component. They operate by opening very low currents, but a smaller hybrid device can be designed if they are faster at opening their contacts. The proposed solution is a step forward for the existing hybrid solutions because it is the first one that allows both normal and short-circuit operations without damage or extra aging of the device.

References

[1] J. J. Justo, F. Mwasilu, J. Lee, and J. Jung, "AC-microgrids versus DC-microgrids with distributed energy resources: A review," *Renewable Sustain. Energy Rev.*, vol. 24, pp. 387–405, Aug. 2013.

[2] T. Kaipia, P. Salonen, J. Lassila, and J. Partanen, "Application of low voltage DC-distribution system—A techno-economical study," in *Proc. Int. Conf. Exhib. Electricity Distrib.*, 2007, pp. 1–4.

[3] M. E. Baran and N. R. Mahajan, "DC distribution for industrial systems: Opportunities and challenges," *IEEE Trans. Ind. Appl.*, vol. 39, no. 6, pp. 1596–1601, Nov./Dec. 2003.

[4] P. Nuutinen *et al.*, "Experiences from use of an LVDC system in public electricity distribution," in *Proc. 22nd Int. Conf. Exhib. Electricity Distrib.*, 2013, pp. 1–4.

[5] S. Grillo, V. Musolino, L. Piegari, E. Tironi, and C. Tornelli, "DC islands in AC smart grids," *IEEE Trans. Power Electron.*, vol. 29, no. 1, pp. 89–98, Jan. 2014.

[6] T. Dragicevic, J. C. Vasquez, J. M. Guerrero, and D. Skrlec, "Advanced LVDC electrical power architectures and microgrids: A step toward a new generation of power distribution networks," *IEEE Electrific. Mag.*, vol. 2, no. 1, pp. 54–65, Mar. 2014.

[7] R. M. Cuzner and G. Venkataramanan, "The status of DC micro-grid protection," in *Proc. Ind. Appl. Soc. Annu. Meeting*, 2008, pp. 1–8.

[8] A. A. S. Emhemed and G. M. Burt, "An advanced protection scheme for enabling an LVDC last mile distribution network," *IEEE Trans. Smart Grid*, vol. 5, no. 5, pp. 2602–2609, Sep. 2014.

[9] D. Salomonsson, L. Soder, and A. Sannino, "Protection of low-voltage DC microgrids," *IEEE Trans. Power Del.*, vol. 24, no. 3, pp. 1045–1053, Jul. 2009.

[10] A. Emhemed and G. Burt, "The effectiveness of using IEC61660 for characterising short-circuit currents of future low voltage DC distribution networks," in *Proc. Int. Conf. Exhib. Electricity Distrib.*, Stockholm, Sweden, Jun. 2013, pp. 1–4.

[11] W. Rieder, "Circuit breakers physical and engineering problems I—Fundamentals," *IEEE Spectr.*, vol. 7, no. 7, pp. 35–43, Jul. 1970.

[12] W. Rieder, "Circuit breakers physical and engineering problems II—Design considerations," *IEEE Spectr.*, vol. 7, no. 8, pp. 90–94, Aug. 1970.

[13] W. Rieder, "Circuit breakers physical and engineering problems III—Arc-medium considerations," *IEEE Spectr.*, vol. 7, no. 9, pp. 80–84, Sep. 1970.

[14] M. Farhadi and O. A. Mohammed, "Protection of multi-terminal and distributed DC systems: Design challenges and techniques," *Elect. Power Syst. Res.*, vol. 143, pp. 715–727, 2017.

[15] H. Pugliese and M. von Kannewurff, "Discovering DC: A primer on dc circuit breakers, their advantages, and design," *IEEE Ind. Appl. Mag.*, vol. 19, no. 5, pp. 22–28, Sep./Oct. 2013.

[16] C. Meyer, S. Schroder, and R. W. De Doncker, "Solid-state circuit breakers and current limiters for medium-voltage systems having distributed power systems," *IEEE Trans. Power Electron.*, vol. 19, no. 5, pp. 1333–1340, Sep. 2004.
[17] F. Liu, W. Liu, X. Zha, H. Yang, and K. Feng, "Solid-state circuit breaker snubber design for transient overvoltage suppression at bus fault interruption in low-voltage DC microgrid," *IEEE Trans. Power Electron.*, vol. 32, no. 4, pp. 3007–3021, Apr. 2017.
[18] J. Magnusson, R. Saers, L. Liljestrand, and G. Engdahl, "Separation of the energy absorption and overvoltage protection in solid-state breakers by the use of parallel varistors," *IEEE Trans. Power Electron.*, vol. 29, no. 6, pp. 2715–2722, Jun. 2014.
[19] A. M. S. Atmadji and J. G. J. Sloot, "Hybrid switching: A review of current literature," in *Proc. Int. Conf. Energy Manage. Power Del.*, 1998, vol. 2, pp. 683–688.
[20] A. Shukla and G. D. Demetriades, "A survey on hybrid circuit-breaker topologies," *IEEE Trans. Power Del.*, vol. 30, no. 2, pp. 627–641, Apr. 2015.
[21] B. Roodenburg, A. Taffone, E. Gilardi, S. M. Tenconi, B. H. Evenblij, and M. A. M. Kaanders, "Combined ZVS–ZCS topology for high-current direct current hybrid switches: Design aspects and first measurements," *IET Elect. Power Appl.*, vol. 1, no. 2, pp. 183–192, Mar. 2007.
[22] C. M. Franck, "HVDC circuit breakers: A review identifying future research needs," *IEEE Trans. Power Del.*, vol. 26, no. 2, pp. 998–1007, Apr. 2011.
[23] P. J. Theisen, S. Krstic, and C. Chen, "270-V DC hybrid switch," *IEEE Trans. Compon., Hybrids, Manuf. Technol.*, vol. CHMT-9, no. 1, pp. 97–100, Mar. 1986.
[24] J. M. Meyer and A. Rufer, "A DC hybrid circuit breaker with ultra-fast contact opening and integrated gate-commutated thyristors (IGCTs)," *IEEE Trans. Power Del.*, vol. 21, no. 2, pp. 646–651, Apr. 2006.
[25] S. Roy, D. Kanabar, C. Dodiya, and S. Pradhan, "Development of a prototype hybrid DC circuit breaker for superconducting magnets quench protection," *IEEE Trans. Appl. Supercond.*, vol. 24, no. 6, Dec. 2014, Art. no. 4702006.
[26] D. Keshavarzi, E. Farjah, and T. Ghanbari, "Hybrid DC circuit breaker and fault current limiter with optional interruption capability," *IEEE Trans. Power Electron.*, vol. 33, no. 3, pp. 2330–2338, Mar. 2018.
[27] A. Hassanpoor, J. Häfner, and B. Jacobson, "Technical assessment of load commutation switch in hybrid HVDC breaker," *IEEE Trans. Power Electron.*, vol. 30, no. 10, pp. 5393–5400, Oct. 2015.
[28] X. Song, C. Peng, and A. Q. Huang, "A medium-voltage hybrid DC circuit breaker, part I: Solid-state main breaker based on 15 kV SiC emitter turn-off thyristor," *IEEE J. Emerg. Sel. Topics Power Electron.*, vol. 5, no. 1, pp. 278–288, Mar. 2017.
[29] C. Peng, X. Song, A. Q. Huang, and I. Husain, "A medium-voltage hybrid DC circuit breaker—part II: Ultrafast mechanical switch," *IEEE J. Emerg. Sel. Topics Power Electron.*, vol. 5, no. 1, pp. 289–296, Mar. 2017.
[30] J. Zyborski, T. Lipski, J. Czucha, and S. Hasan, "Hybrid arcless low-voltage AC/DC current limiting interrupting device," *IEEE Trans. Power Del.*, vol. 15, no. 4, pp. 1182–1187, Oct. 2000.
[31] T. G. Hailu, L. Mackay, L. M. Ramirez-Elizondo, and J. A. Ferreira, "Voltage weak DC distribution grids," *Elect. Power Compon. Syst.*, vol. 45, no. 10, pp. 1091–1105, 2017.
[32] S. Anand and B. G. Fernandes, "Reduced-order model and stability analysis of low-voltage DC microgrid," *IEEE Trans. Ind. Electron.*, vol. 60, no. 11, pp. 5040–5049, Nov. 2013.
[33] D. Jovcic, W. Lin, S. Nguefeu, and H. Saad, "Low-energy protection system for DC grids based on full-bridge MMC converters," *IEEE Trans. Power Del.*, vol. 33, no. 4, pp. 1934–1943, Aug. 2018.
[34] C. Peng, I. Husain, A. Q. Huang, B. Lequesne, and R. Briggs, "A fast mechanical switch for medium-voltage hybrid DC and AC circuit breakers," *IEEE Trans. Ind. Appl.*, vol. 52, no. 4, pp. 2911–2918, Jul./Aug. 2016.
[35] M. A. Sanchez, "Dynamics of an ultra-fast Thomson-actuated HVDC breaker," M.Sc. thesis, Ind. Eng. Manage., KTH Roy. Inst. Technol., Stockholm, Sweden, Jun. 2017. [Online]. Available: https://kth.diva-portal.org/smash/get/diva2:1113124/FULLTEXT01.pdf, Accessed on: Jun. 19, 2018.
[36] D. Ronchegalli and R. Lazzari, "Development of the control strategy for a direct current microgrid: A case study," in *Proc. AEIT Int. Annu. Conf.*, Capri, Italy, 2016, pp. 1–6.
[37] F. F. Wang and Z. Zhang, "Overview of silicon carbide technology: Device, converter, system, and application," *CPSS Trans. Power Electron. Appl.*, vol. 1, no. 1, pp. 13–32, Dec. 2016.
[38] [Online]. Available: http://www.te.com/commerce/DocumentDelivery/DDEController?Action=srchrtrv&DocNm=5-1773450-5_Section7&DocType=CS&DocLang=EN, Accessed on: Jun. 1, 2018.

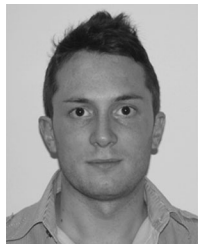

Riccardo Lazzari received the M.S. degree in electronic engineering from the Politecnico di Milano, Milan, Italy, in 2009.

Since 2009, he has been with the Power Generation Technologies and Materials Department, Ricerca sul Sistema Energetico S.p.A., Milan, Italy, as a Research Engineer. He has acquired a wide experience in project development and experimentation of test facilities, and in particular on microgrid's control system development. He is involved in national and EU research projects on smart grids and renewable power system. His research interests include analysis, modeling, and control of power converters and low-voltage dc grids.

Luigi Piegari (M'04–SM'13) was born in Naples, Italy, on April 2, 1975. He received the M.S. (*cum laude*) and Ph.D. degrees in electrical engineering from the University of Naples Federico II, Naples, Italy, in 1999 and 2003, respectively.

From 2003 to 2008, he was a Postdoctoral Research Fellow with the Department of Electrical Engineering, University of Naples Federico II. From 2009 to 2012, he was an Assistant Professor with the Department of Electrical Engineering, Polytechnic University of Milan, Milan, Italy. He is currently an Associate Professor of electrical machines and drives with the Department of Electronics, Information and Bioengineering, Polytechnic University of Milan. He is the author of more than 100 scientific papers published in international journals and conference proceedings. His research interests include storage devices modeling, wind and photovoltaic generation, modeling and control of multilevel converters, and dc distribution grids.

Prof. Piegari is a member of the IEEE Industrial Electronics Society, the IEEE Power Electronics Society, and the AEIT. He is the Technical Program Chair of the International Conference on Clean Electrical Power.